CHAPTER 4

RESULTS AND DISCUSSIONS

This study employs a constitutive equation and associates with three material parameters sets for three-layer murine aortic wall in the new mechanical modeling and two constitutive equations and associates with five material parameters sets for five-layer human aortic wall in three-dimension model based on *in vivo* non-invasive experimental data in the new mechanical modeling. So, we attempt to verify our computational model with a number of exist studies of one-layer and two-layer material models by using their constitutive equations and material parameters sets in our computational program. These comparisons with previous studies are demonstrated in Section 4.1. The model is then used to determine stresses and strains distributions of murine aortic vessel in three-dimension three-layer abdominal aortic wall based on *in vivo* ultrasound imaging and stresses and strains distributions of human aortic vessel in three-dimension five-layer aortic wall based on *in vivo* ultrasound imaging which results and discussion are expressed in Section 4.2 and 4.3, respectively. Effect of pressure on aortic walled rupture of human aortic vessel in three-dimension five-layer aortic wall based on *in vivo* ultrasound imaging is also examined and show results and discussion in Section 4.4.

4.1. Comparisons with previous studies

There are a list of nine cases of number of layer, source of comparison, constitutive equation and utilized parameters in Table 4.1. From Figure 4.1 through Figure 4.4, there are four cases of one-layer model computed by our computational program for relationships of inside radius and luminal pressure (Cases 1A, 1B), relationship of luminal pressure and outside radius (Case 1C) and relationship of outside diameter and luminal pressure (Case 1D).

In Figure 4.5 through Figure 4.9, there are five cases of two-layer model computed by our computational program for relationships of inside radius and luminal pressure (Case 2A), principal Cauchy stresses across arterial wall (Case 2B), relationship of outside diameter and luminal pressure (Case 2C) and relationship of luminal pressure and outside radius (Cases 2D, 2E). The solutions are found to be in good agreement with previous studies by square of Pearson product moment correlations, r_d, between dependences of present study and previous studies are more than 0.98 in all cases (1A-1D and 2A-2E). Slight different of the results also might occur because of the method for solving the equations that is not reported in their literatures.

The computational program is extend to calculate the solutions in our both mechanical model for stresses and strains distributions of murine aortic vessel in three-dimension three-layer abdominal aortic wall based on *in vivo* ultrasound imaging and stresses and strains distributions of human aortic vessel in three-dimension five-layer aortic wall based on *in vivo* ultrasound imaging and consequently the results are analyzed for rupture of arterial wall.

Table 4.1 The list of number of layer, source of comparison, constitutive equation and utilized parameters for comparison our computational model

Figure	Case	Number of layers	Source of comparison	Constitutive equation	Utilized parameters
4.1	1 A	1	Holzapfel *et al.* (2000)	Delfino *et al.* (1997)	Artery; a = 44.2 kPa, b = 16.7
4.2	1 B	1	Holzapfel *et al.* (2000)	Fung's type	Artery; c = 26.95 kPa, b_1 =0.9925, b_2 = 0.4180, b_3 = 0.0089, b_4 = 0.0749, b_5 = 0.029, b_6 = 0.0193, b_7 = 5.000
4.3	1 C	1	Sokolis (2010)	Fung's type	Esophagus; c = 2.0934 kPa, b_1 =0.783, b_2 = 7.385, b_4 = 0.611
4.4	1 D	1	von Maltzahn *et al.* (1984)	Fung's type	Artery; c = 2.4657*2 kPa, b_1 = 0.1499, b_2 = 1.6409, b_4 = 0.0028/2
4.5	2 A	2	Holzapfel *et al.* (2000)	Holzapfel *et al.* (2000)	Media; c = 3.000 kPa, k_1 = 2.3632 kPa, k_2 = 0.8393 Adventitia; c = 0.3000 kPa, k_1 = 0.5620 kPa, k_2 = 0.7112
4.6	2 B	2	Holzapfel *et al.* (2000)	Holzapfel *et al.* (2000)	Media; c = 3.000 kPa, k_1 = 2.3632 kPa, k_2 = 0.8393 Adventitia; c = 0.3000 kPa, k_1 = 0.5620 kPa, k_2 = 0.7112
4.7	2 C	2	von Maltzahn *et al.* (1984)	Fung's type	Media; c = 2.4657*2 kPa, b_1 =0.1499, b_2 = 1.6409, b_4 = 0.0028/2 Adventitia; c = 9.1140*2 kPa, b_1 =0.1939, b_2 = 1.2601, b_4 = 0.7759/2
4.8	2 D	2	Sokolis (2010)	Fung's type	Mucosa-submucosa; c = 2406.1 Pa, b_1 =2.220, b_2 = 10.229, b_4 = 1.747 Muscle; c = 1012.6 Pa, b_1 =0.568, b_2 = 5.197, b_4 = 0.360
4.9	2 E	2	Sokolis (2010)	Fung's type	Mucosa-submucosa; c = 1974.4 Pa, b_1 =3.296, b_2 = 11.529, b_4 = 1.847 Muscle; c = 1012.6 Pa, b_1 =0.568, b_2 = 5.197, b_4 = 0.360

Note: Strain energy function of Delfino *et al*. (1997), $\bar{\Psi} = \frac{a}{b}\left\{\exp\left[\frac{b}{2}(\bar{I}_1 - 3)\right] - 1\right\}$

Strain energy function of Fung's type, $\bar{\Psi} = \frac{1}{2}c\{\exp(\bar{Q}) - 1\}$,

$$\bar{Q} = b_1\bar{E}_{\Theta\Theta}^2 + b_2\bar{E}_{ZZ}^2 + b_3\bar{E}_{RR}^2 + 2b_4\bar{E}_{\Theta\Theta}\bar{E}_{ZZ} + 2b_5\bar{E}_{ZZ}\bar{E}_{RR} + 2b_6\bar{E}_{RR}\bar{E}_{\Theta\Theta} + b_7\bar{E}_{\Theta Z}^2 + b_8\bar{E}_{RZ}^2 + b_9\bar{E}_{R\Theta}^2$$

Strain energy function of Holzapfel *et al*. (2000), $\bar{\Psi} = \frac{1}{2}c(\bar{I}_1 - 3) + \frac{k_1}{2k_2}\sum_{i=4,6}\{\exp[k_2(\bar{I}_1 - 1)^2] - 1\}$

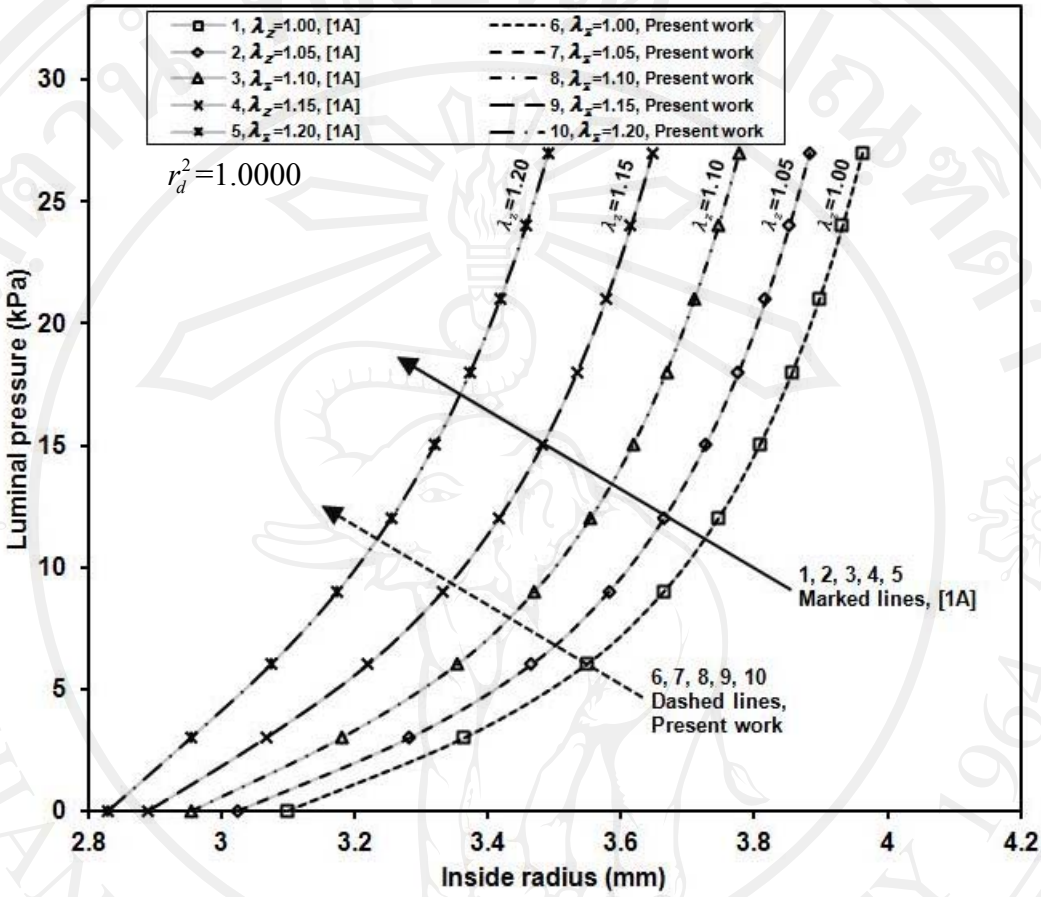

Figure 4.1 Comparison result, inside radius and luminal pressure relationship by using Delfino *et al.* (1997) constitutive equation for one-layer artery (Case 1A)

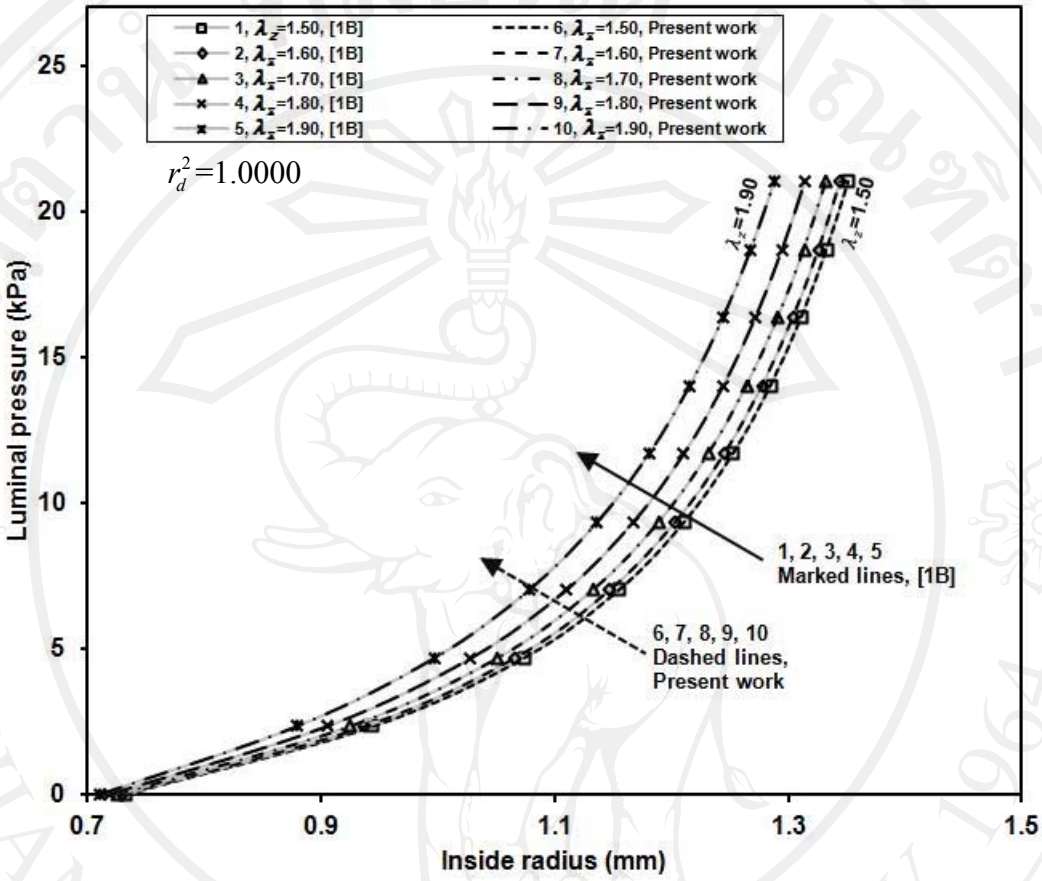

Figure 4.2 Comparison result, inside radius and luminal pressure relationship by using Fung's type constitutive equation for one-layer artery (Case 1B)

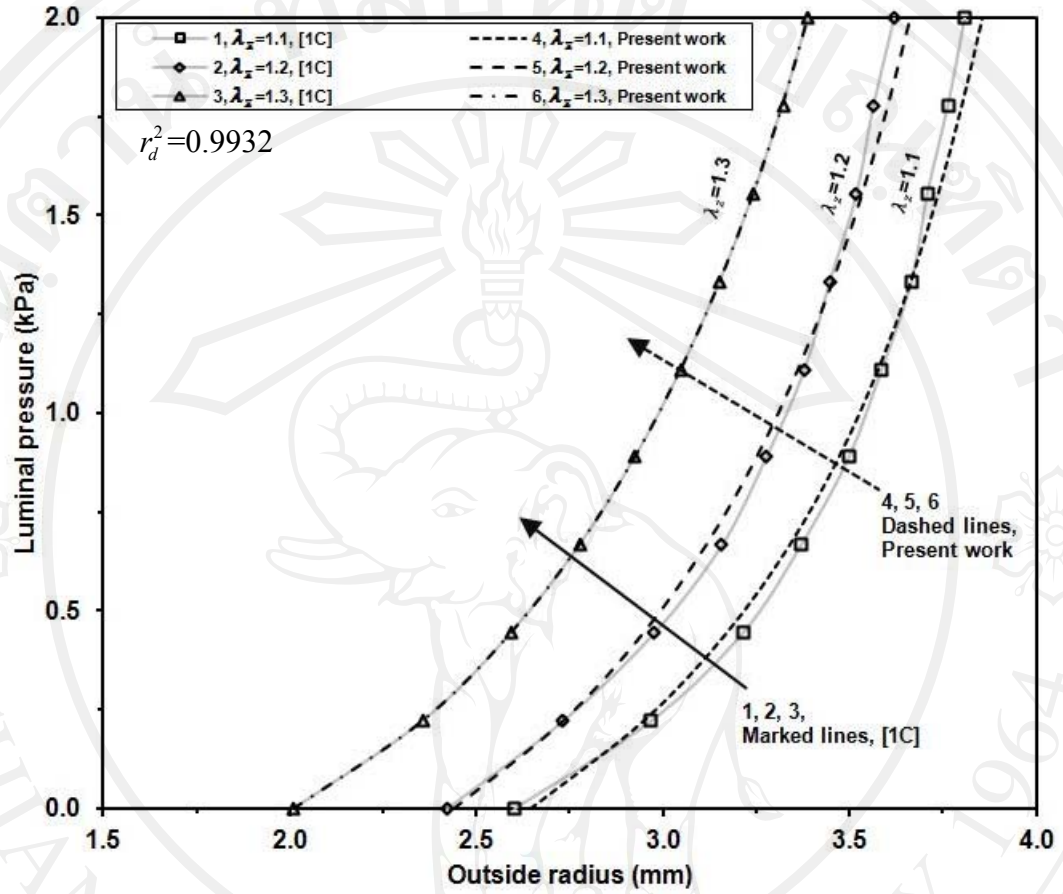

Figure 4.3 Comparison result, outside radius and luminal pressure relationship by using Fung's type constitutive equation for one-layer esophageal wall (Case 1C)

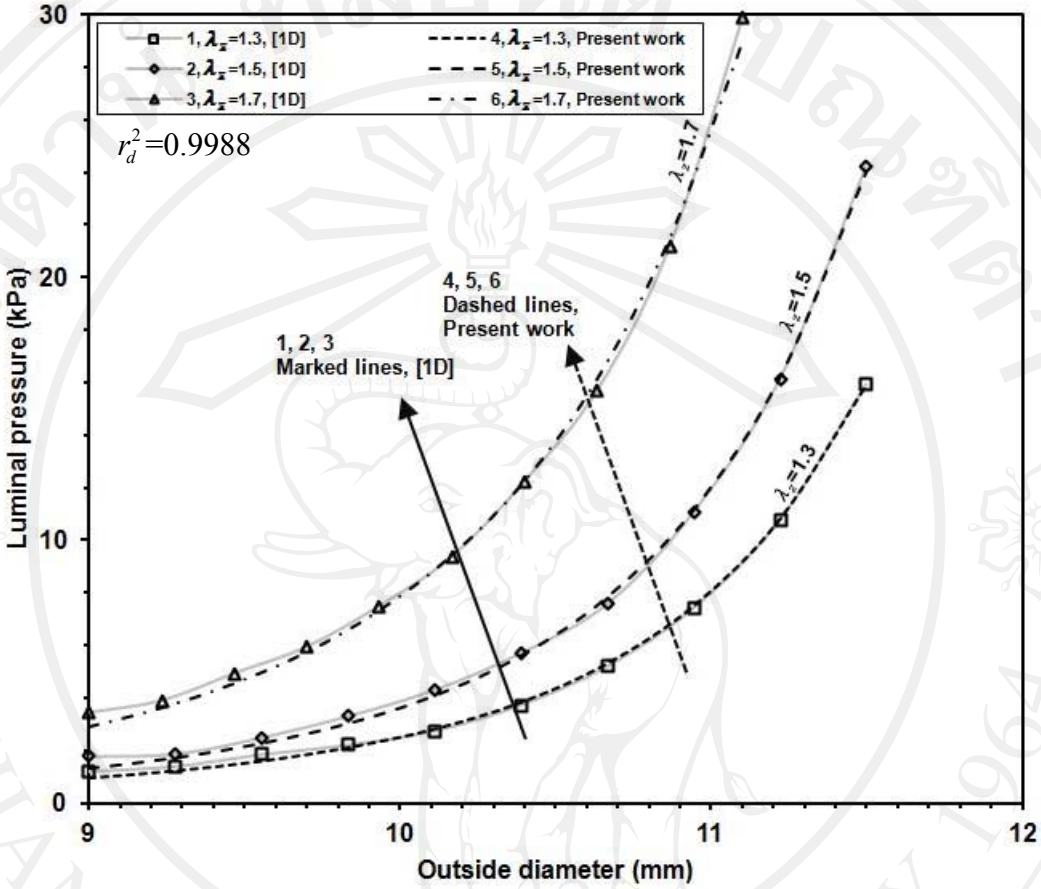

Figure 4.4 Comparison result, outside diameter and luminal pressure relationship by using Fung's type constitutive equation for one-layer esophageal wall (Case 1D)

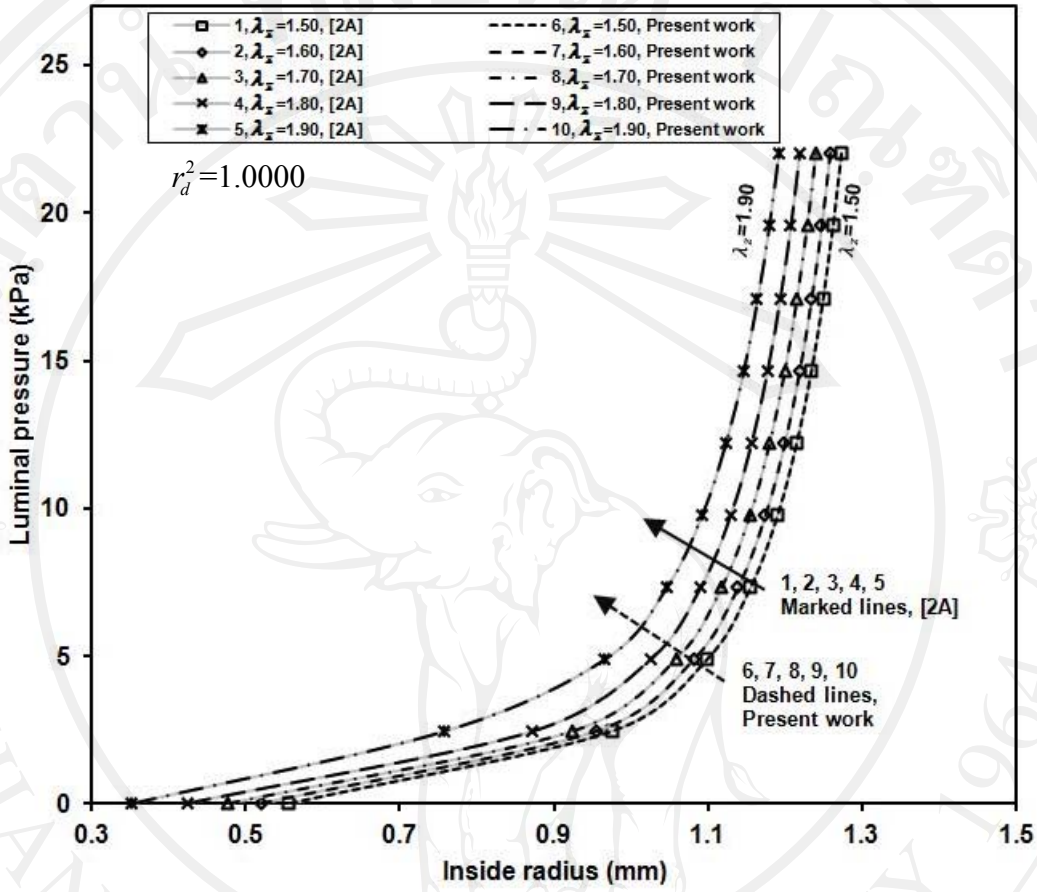

Figure 4.5 Comparison of inside radius and luminal pressure relationship by using Holzapfel *et al.* (2000) constitutive equation for two-layer artery (Case 2A)

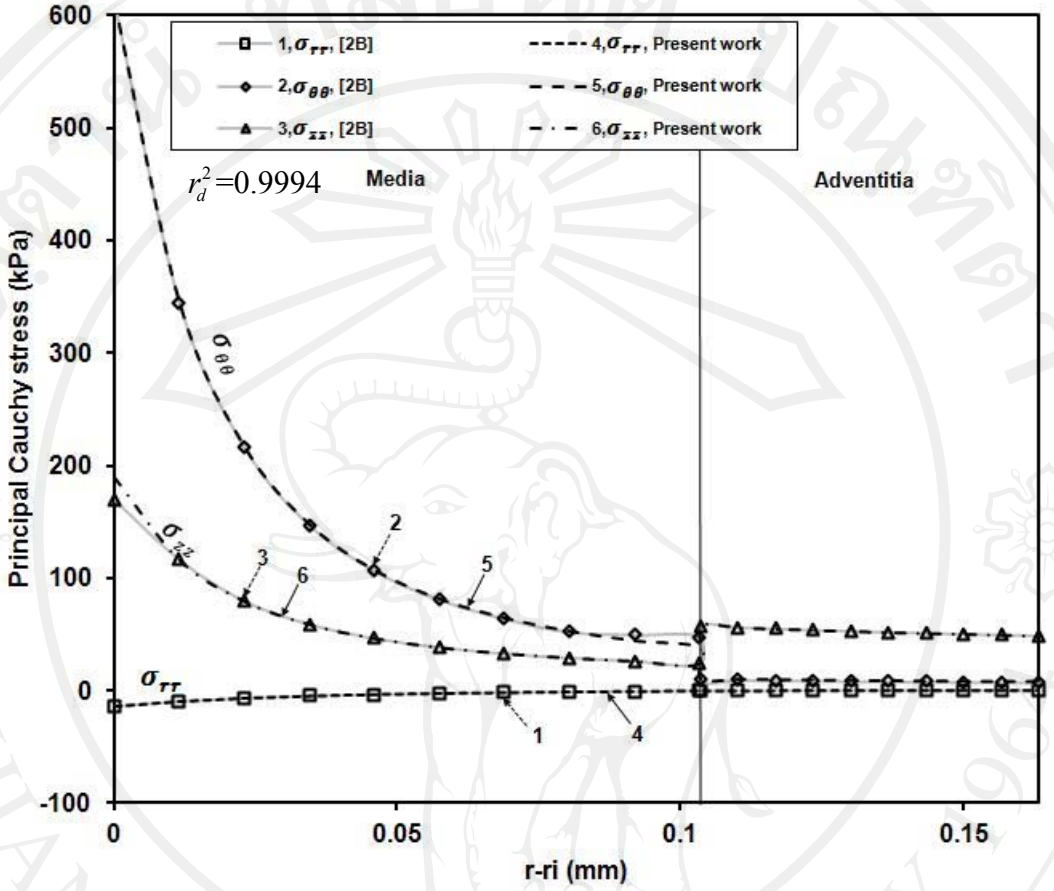

Figure 4.6 Comparison of principal Cauchy stresses across arterial wall at mean pressure by using Holzapfel *et al.* (2000) constitutive equation for two-layer artery (Case 2B)

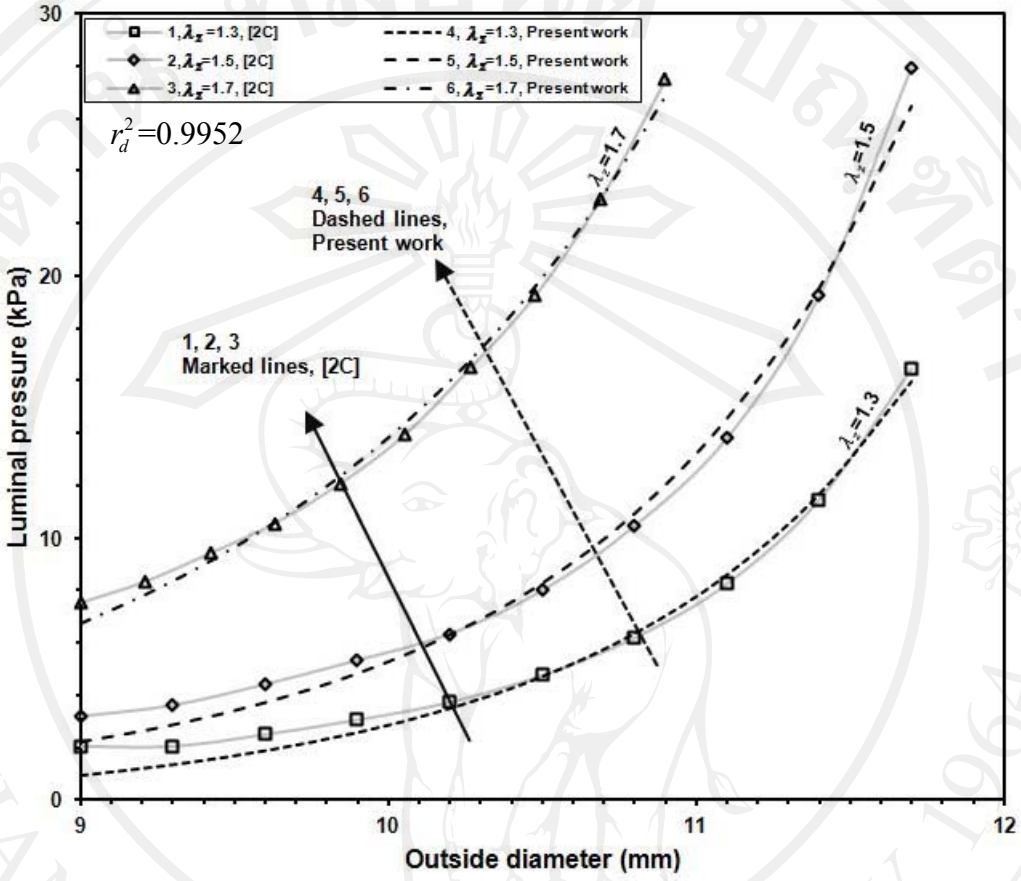

Figure 4.7 Comparison of outside diameter and luminal pressure relationship by using Fung's type constitutive equation for two-layer carotid artery (Case 2C)

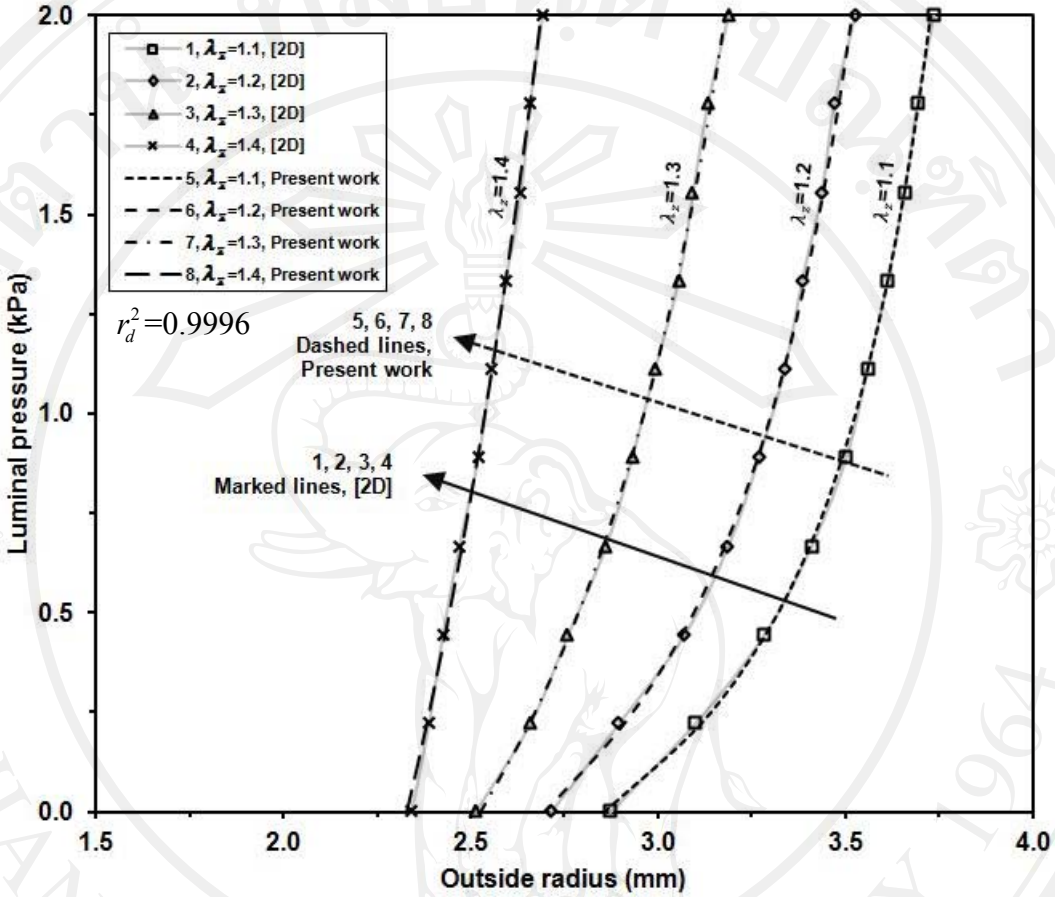

Figure 4.8 Comparison of luminal pressure and outside radius relationship by using Fung's type constitutive equation for two-layer esophageal wall (Case 2D)

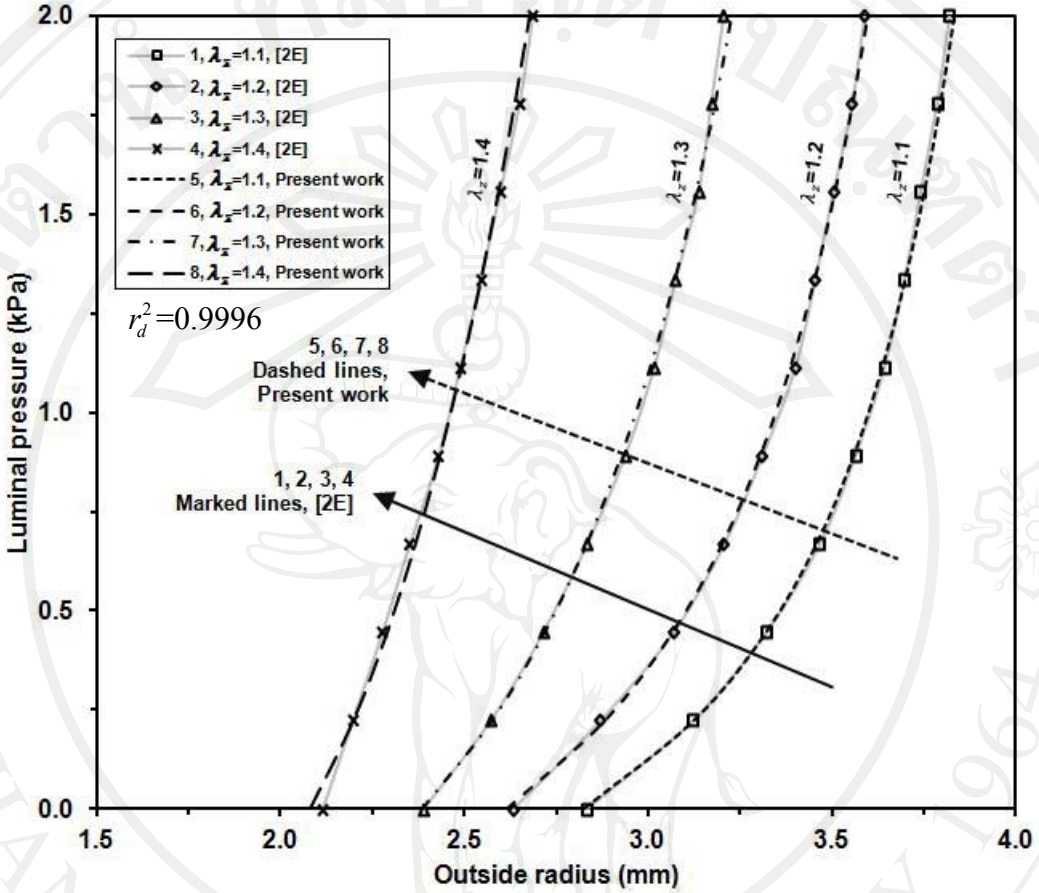

Figure 4.9 Comparison of outside radius and luminal pressure relationship by using Fung's type constitutive equation for two-layer esophageal wall (Case 2E)

In addition, our computational model is examined by comparing with experimental data at carotid artery (von Maltzahn *et al.*, 1984) as shown in Figure 4.10. Fung's type constitutive equation for two-layer carotid artery is used. Two parameter sets from previous work (von Maltzahn *et al.*, 1984) and present work are presented in Table 4.2.

Table 4.2 Two parameter sets of previous work (von Maltzahn *et al.*, 1984) and present work by using Fung's type constitutive equation for two-layer carotid artery

Source of comparison	Utilized parameters	$\sqrt{MSE}$	r_d^2
von Maltzahn *et al.* (1984)	Media; c = 2.4657*2 kPa, b_1 =0.1499, b_2 = 1.6409, b_4 = 0.0028/2 Adventitia; c = 9.1140*2 kPa, b_1 =0.1939, b_2 = 1.2601, b_4 = 0.7759/2	1.1385 kPa	0.9092
Present work	Media; c = 1.1634*2 kPa, b_1 =0.0624, b_2 =1.0690, b_4 = 0.0036/2 Adventitia; c = 20.2399*2 kPa, b_1 =0.3095, b_2 =1.8366, b_4 = 0.0461/2	0.0652 kPa	0.9635

Using parameter set obtained in present work, consistent of the model and experimental data (von Maltzahn *et al.*, 1984) is presented. While root of minimizes function of mean square error of pressures is 1.1385 kPa in previous work (von Maltzahn *et al.*, 1984), that root of minimizes function of mean square error of 0.0652 kPa is obtained in present work. Moreover, square of correlation coefficient between previous work (von Maltzahn *et al.*, 1984) and experimental data is 0.9092. Greater value of that square of correlation coefficient of 0.9635 is obtained is this study.

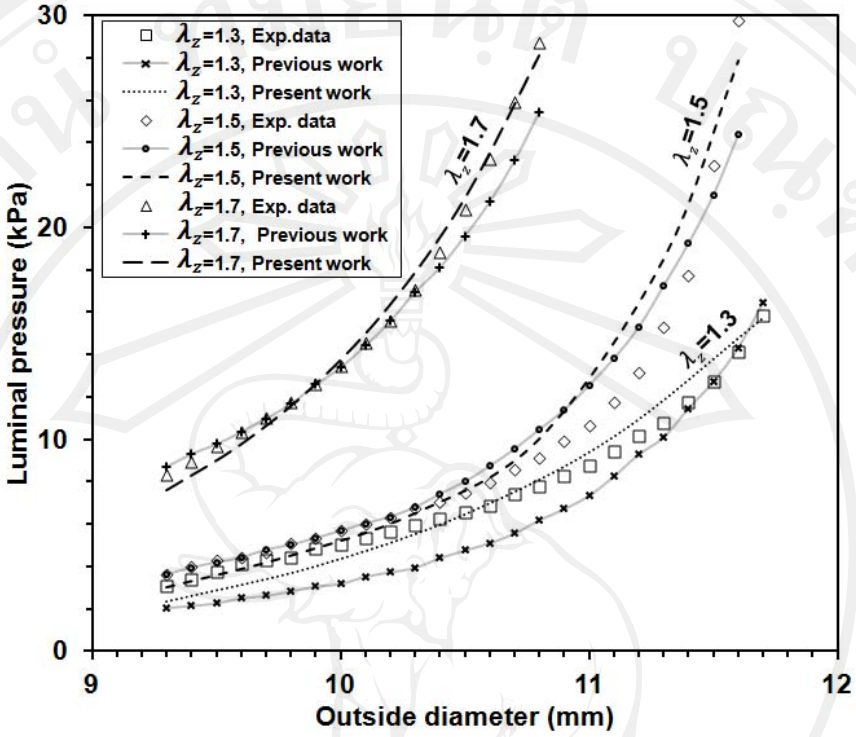

Figure 4.10 Comparison between experimental data (von Maltzahn *et al.,* 1984) and results obtained from two parameter sets of previous work (von Maltzahn *et al.,* 1984) and present work by using Fung's type constitutive equation for two-layer carotid artery

4.2. Stresses and strains distributions of murine aortic vessel in three-dimension three-layer abdominal aortic wall based on *in vivo* ultrasound imaging

4.2.1. Parameter estimation

Material parameter cannot be arbitrarily chosen. Figure 4.11 show contour plot of the potential in adventitia layer of mouse#061 with parameter set in Table 4.3, as an example. If the contour is non-convexity, the physical meanings of parameters are not clear. Thus, it is important to perform optimization process within the range which convexity exists. The material parameters and heart rate data of five healthy mice show in Table 4.3 where HR denotes heart rate, N denotes number of data positions along longitudinal direction and r_{par} denotes correlation coefficient.

Table 4.3 Material parameters and heart rate data of murine abdominal aortas

Mouse		#061	#132	#133	#140	#301	Average	STD
HR,[bpm]		465	472	409	434	483	453	30.4187
N, [position]		89	42	11	28	10	-	-
Intima	β, [deg]	9	10	5	30	24	16	11
	c, [kPa]	10.5318	10.4917	17.1348	17.0012	37.3718	18.5063	11.0440
	k_1, [kPa]	2.0523	2.0826	2.3094	1.7824	1.7420	1.9938	0.2340
	k_2, [-]	1.1767	1.2018	1.2412	1.7915	0.1931	1.1209	0.5777
Media	β, [deg]	10	10	7	15	15	11	4
	c, [kPa]	24.1260	24.4554	22.0990	15.5567	34.4000	24.1274	6.7677
	k_1, [kPa]	1.6E-13	1.6E-13	4.6E-14	1.4E-13	2.9E-13	1.6E-13	8.8E-14
	k_2, [-]	11.8575	11.9015	11.9443	12.1312	11.2708	11.8211	0.3248
Adventitia	β, [deg]	20	20	13	32	15	20	7
	c, [kPa]	2.4126	2.4455	2.2099	1.5557	3.4400	2.4127	0.6768
	k_1, [kPa]	2.3588	2.4728	1.6444	3.9931	0.5971	2.2133	1.2442
	k_2, [-]	3.0747	3.1237	2.9355	3.0976	1.8203	2.8104	0.5582
r_{par}^2		0.9247	0.9287	0.9397	0.9332	0.9651	0.9383	0.0160
$\sqrt{MSE}$ [kPa]		0.5484	0.5609	0.5097	0.5418	0.3828	0.5087	0.0729

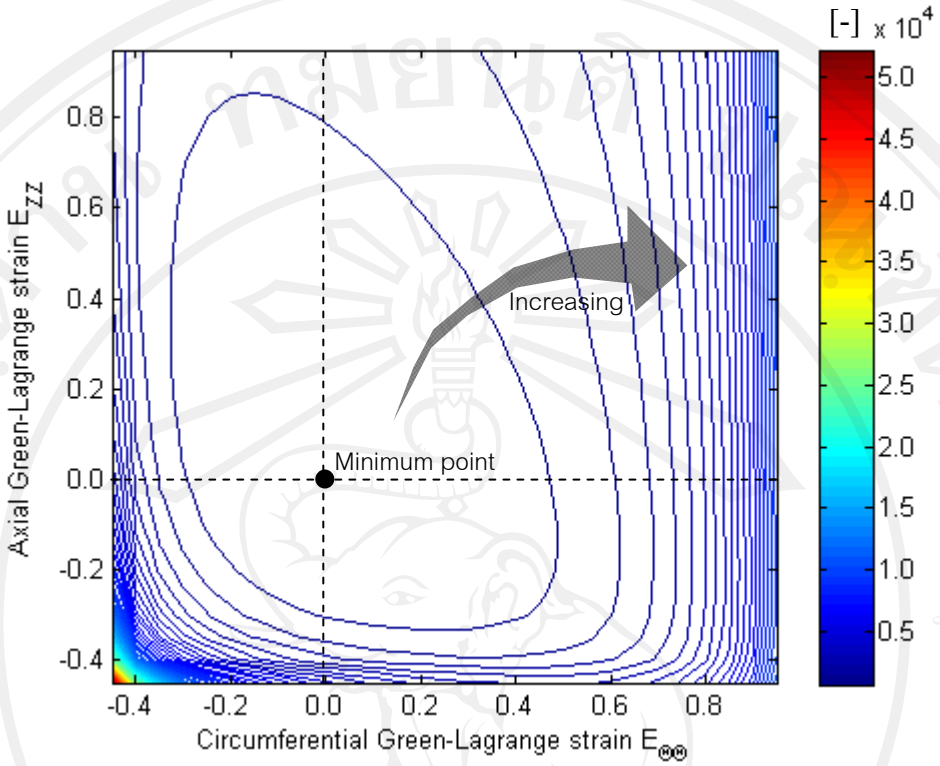

Figure 4.11 Contour of strain energy potential (Pa)

4.2.2. Boundary conditions

Luminal pressure (pressure inside lumen of the artery) and outside pressure are constrains of inside wall and outside wall.

Figures 4.13 through Figure 4.16, results are shown in plane of longitudinal and radial directions as illustrated in Figure 4.12 which is in reference configulation.

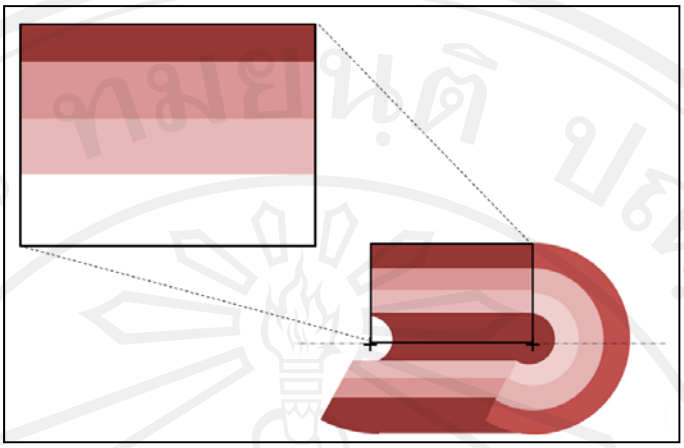

Figure 4.12 Plane of longitudinal and radial directions used to show results in Figure 4.13 through Figure 4.16 for three layers of intima, media and adventitia from inside toward outside of aortic wall.

For instance, Cauchy radial stress distribution in reference configuration of longitudinal distance (N=89 points) across reference intima, media and adventitia layers is illustrated in Figure 4.13 at the physiological state with p_i=82.51 mmHg. This ensures the computational program for three-dimension boundary value problem as following.

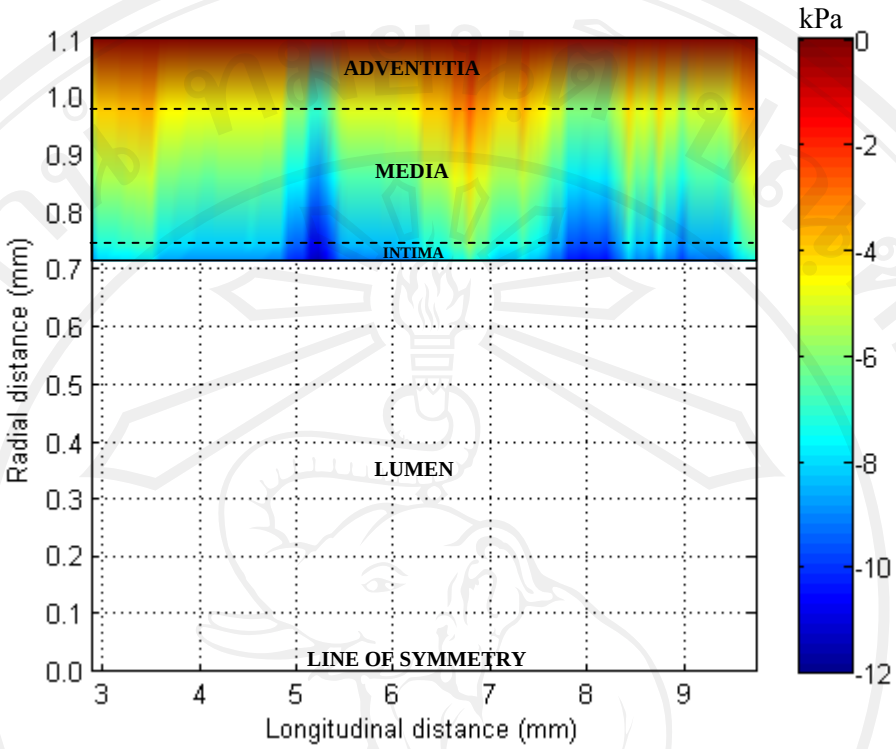

Figure 4.13 Cauchy radial stress (kPa) distribution

At certain longitudinal position, Cauchy radial stress is continuous from inside wall which equal to negative value of luminal pressure and varies from this negative value at the inside wall and is continuous across interfaces of layers (intima-media interface and media-adventitia interface) toward outside pressure at the outside wall. This trend of the variation of radial stress in certain longitudinal position could be also observed in many previous studies (Holzapfel *et al.*, 2000; Holzapfel, 2001; Fung, 1990). Stresses and strains distribution in coordinate of three dimensions and in three major layers of abdominal aortic wall based on *in vivo* ultrasound data could be predicted successfully. To discussions the results, stresses and strains distributions in reference configuration of longitudinal distance across the reference intima, media and adventitia layers from experimental data of mouse#061 and its parameter set is used to interpret as instances in the physiological state with luminal pressure of 82.51

mmHg (dilated phase), longitudinal stretch of 1.7, reference inside and outside radius of 0.71 and 1.1 mm, respectively, without torsion and residual strains. Luminal pressure in cardiac cycle of the experiment varies from 37.50 mmHg at end contraction phase to 90.01 mmHg at end dilated phase. Non uniform value in longitudinal direction occurs because of the non uniform of diameter which are obtained from ultrasound scanning.

4.2.3. Principal Cauchy stresses and Green-Lagrange strains distributions across the arterial wall

The strains distribution in radial and circumferential directions in configuration of longitudinal distance across the reference intima, media and adventitia layer could be illustrated in Figure 4.14 and Figure 4.15, respectively.

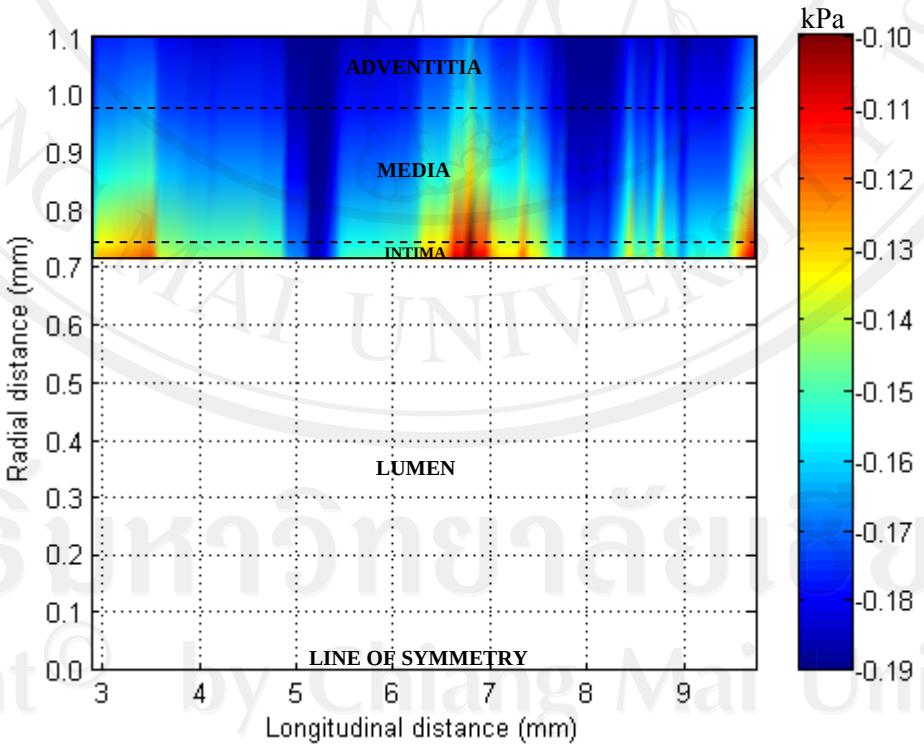

Figure 4.14 Green radial strain distribution

Green radial strain tensor is represented as negative value because this state the vascular has been dilated by luminal pressure. Lumen of the vascular increases while conservation of volume, thickness of this state is reduced resulting to radial strain is negative.

Green longitudinal strain is equal to 0.945 for all positions because of no torsion. The continuous of strains at both of interfaces, intima-media interface and media-adventitia interface, is found because continuous body of vascular is assumed.

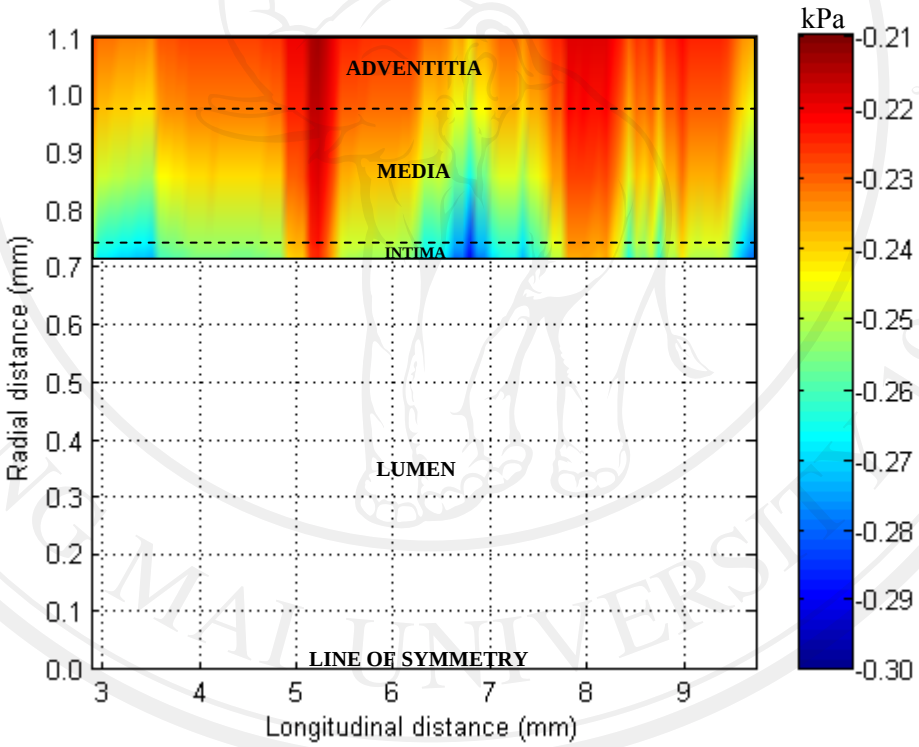

Figure 4.14 Green circumferential strain distribution

The stresses distribution in radial, circumferential and longitudinal directions in configuration of longitudinal distance across the reference intima, media and adventitia layer could be illustrated in Figure 4.13, Figure 4.16 and Figure 4.17, respectively. In contrast to Cauchy radial stress distribution, Cauchy stress

distributions in circumferential, longitudinal directions are discontinuous at both of interfaces, intima-media interface and media-adventitia interface. The behavior shown in Figure 4.16 is similar to that found by Holzapfel *et al.* (2000) by following. It could be observed that the circumferential stress in media layer has relatively high value compared with the value in adventitia. Extend from two layers of media and adventitia of Holzapfel *et al.* (2000) by intima layer is in to accounted, the relatively highest value of circumferential stress occurs in intima layer. Overall of trend of the magnitude that the highest occurs at inside wall and then decreases toward to outside wall is also found by Fung (1990). Moreover, the magnitude of radial stress is smaller than in others directions.

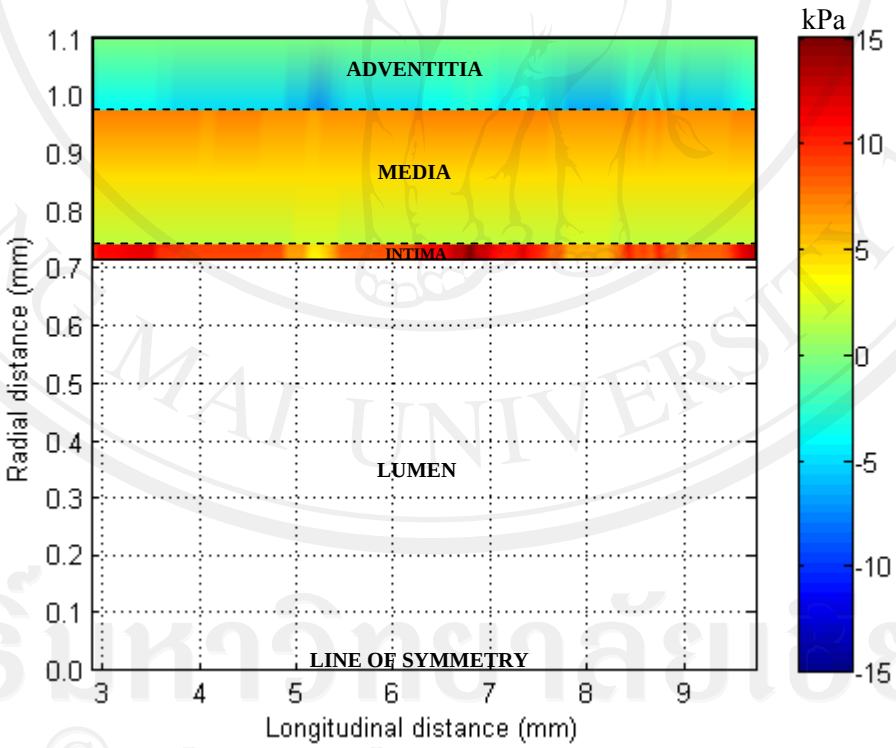

Figure 4.16 Cauchy circumferential stress (kPa) distribution

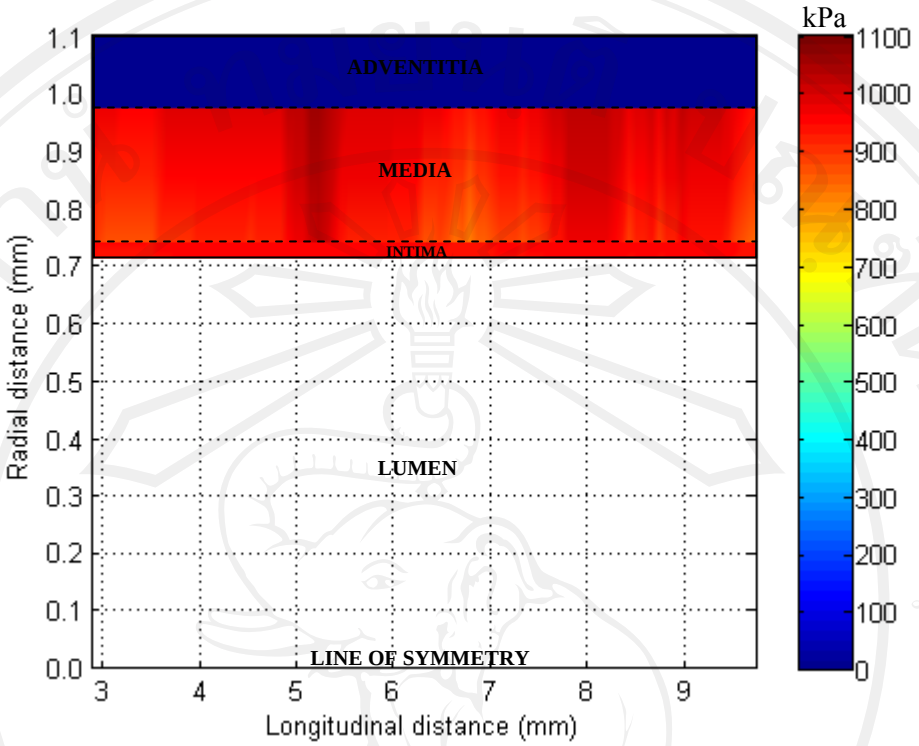

Figure 4.17 Cauchy longitudinal stress (kPa) distribution

4.3. Stresses and strains distributions of human aortic vessel in three-dimension five-layer aortic wall based on *in vivo* ultrasound imaging

4.3.1. Parameter estimation

The mean square error of pressure called 'Objective function' is used to determine the constitutive parameters. The measured luminal pressure and inside diameter by *in vivo* non-invasive experiment are used in five-layer model for minimizing the objective function in this estimation. The estimated parameters could show in Table 4.4 and root of minimizes function of mean square error of pressures of 0.5631 kPa is obtained.

Table 4.4 The estimated parameters

Layer	Optimized parameters		
	c [kPa]	k_1 [kPa]	k_2
Endothelium	250.9108	-	-
Intima	270.9837	2.1492	1.3012
IEL	250.9108	-	-
Media	100.3643	3.5820	5.2049
Adventitia	10.0364	0.0716	0.9759

By these estimated parameters sets, the convexities of strain energy density contour in circumferential and longitudinal directions are investigated and obtained as valley for every arterial layers.

4.3.2. Principal Cauchy stresses and Green-Lagrange strains distributions across the arterial wall

The results of principal Cauchy stresses and Green-Lagrange strains distributions across the deformed arterial wall could be illustrated in Figure 4.19 and Figure 4.20. Figure 4.19 shows principal Cauchy stresses distribution in radial, circumferential and longitudinal directions at DBP, MBP and SBP states and Figure 4.20 shows principal Green-Lagrange strains distributions in the same way. Figure 4.19 and Figure 4.20, results are shown in plane of circumferential and radial directions as illustrated in Figure 4.18b. Figure 4.21 and Figure 4.22, results are shown in plane of longitudinal and radial directions as illustrated in Figure 4.18a which are in deformed configuration.

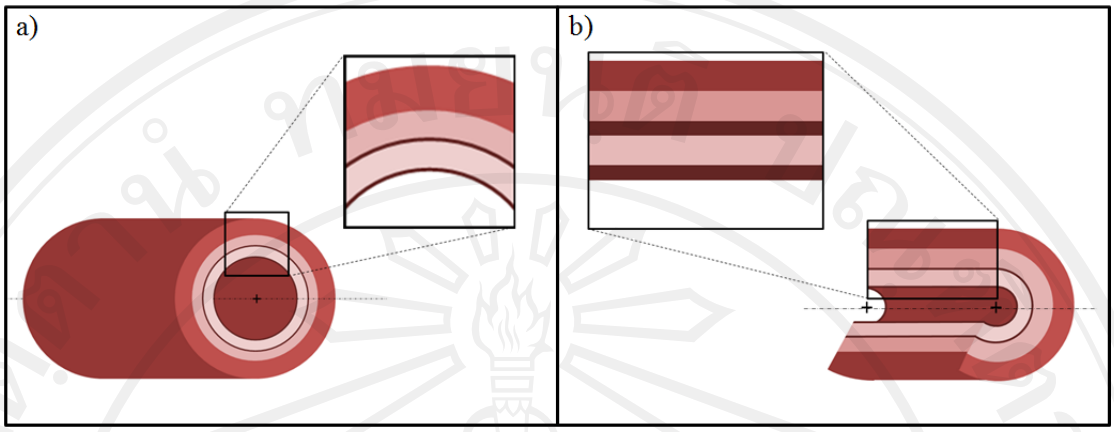

Figure 4.18 a) Plane of circumferential and radial directions used to show results in Figure 4.21 through Figure 4.22 and b) plane of longitudinal and radial directions used to show results in Figure 4.19 through Figure 4.20 for five layers of endothelium, intima, internal elastic lamina, media and adventitia from inside toward outside of aortic wall.

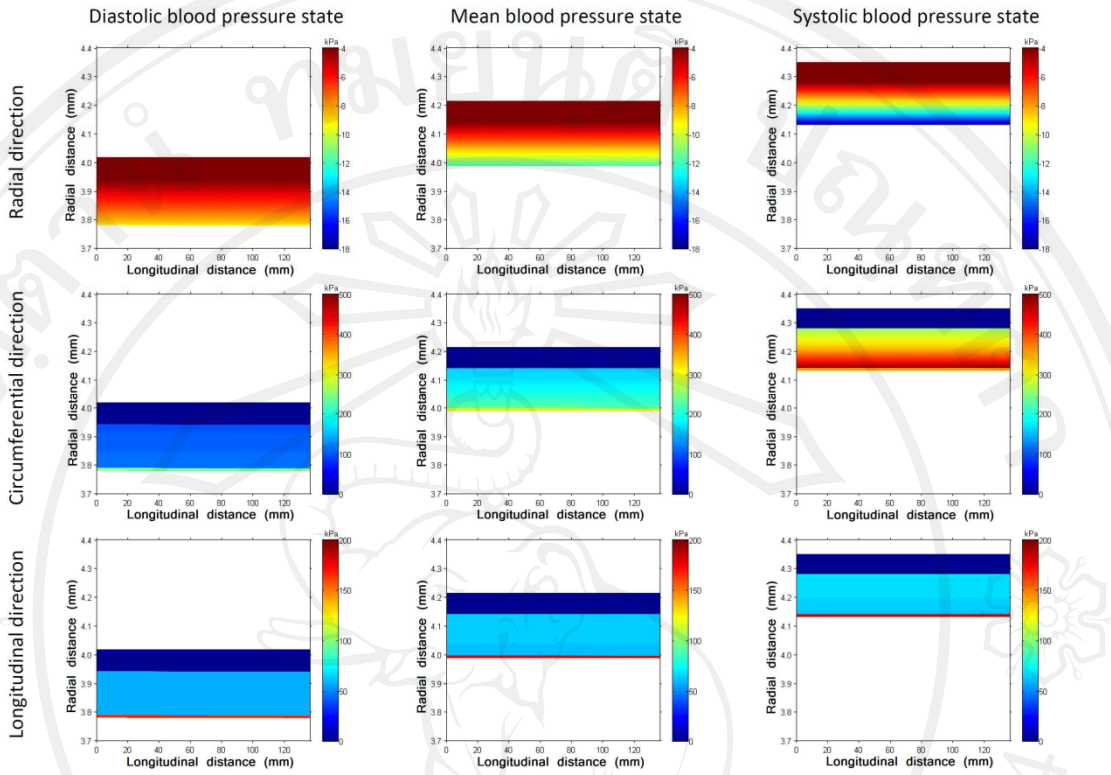

Figure 4.19 Capture images of principal Cauchy stresses distributions across the $r-z$ plane deformed arterial wall in radial direction (1st row), circumferential direction (2nd row) and longitudinal direction (3rd row) at DBP of 69.61 mmHg (1st column), MBP of 89.25 mmHg (2nd column) and SBP of 128.41 mmHg (3rd column) obtained from the model

Boundary conditions are investigated as luminal pressure (pressure inside lumen of the artery) and outside pressure are constrains of inside wall and outside wall. The consistent are obtained that could be seen in Figure 4.19 in the radial stress distributions.

As illustrated in Figure 4.19, magnitudes of principal Cauchy stresses of normal human artery in radial, circumferential and longitudinal directions are in range of 4.00-17.56 kPa, 3.96-493.80 kPa and 2.18-184.56 kPa, respectively. At certain longitudinal position, the Cauchy stress in radial direction is continuous from inside wall which equal to negative value of luminal pressure and varies from this negative value at the inside wall and is continuous across interfaces of layers toward outside pressure at the outside wall. The magnitude of the Cauchy stress in radial direction is smaller than in others directions and the sign of negative means to compressive. In contrast to the Cauchy stress distributions in redial direction, the Cauchy stresses distributions in circumferential and longitudinal directions are discontinuous across the interfaces which because of difference material properties of the layers to resist pressure load. It could be observed the circumferential stress in media layer that the magnitude is relatively high comparing to the adventitia. Extend from two layers of media and adventitia of Reference 1 by endothelium, intima and internal elastic laminar are in to account, the relatively highest magnitude of circumferential stress occurs in intima which is the innermost major layer of arterial wall. Overall of trends of the magnitude present that the highest occurs around inside wall and then decreases toward to outside wall.

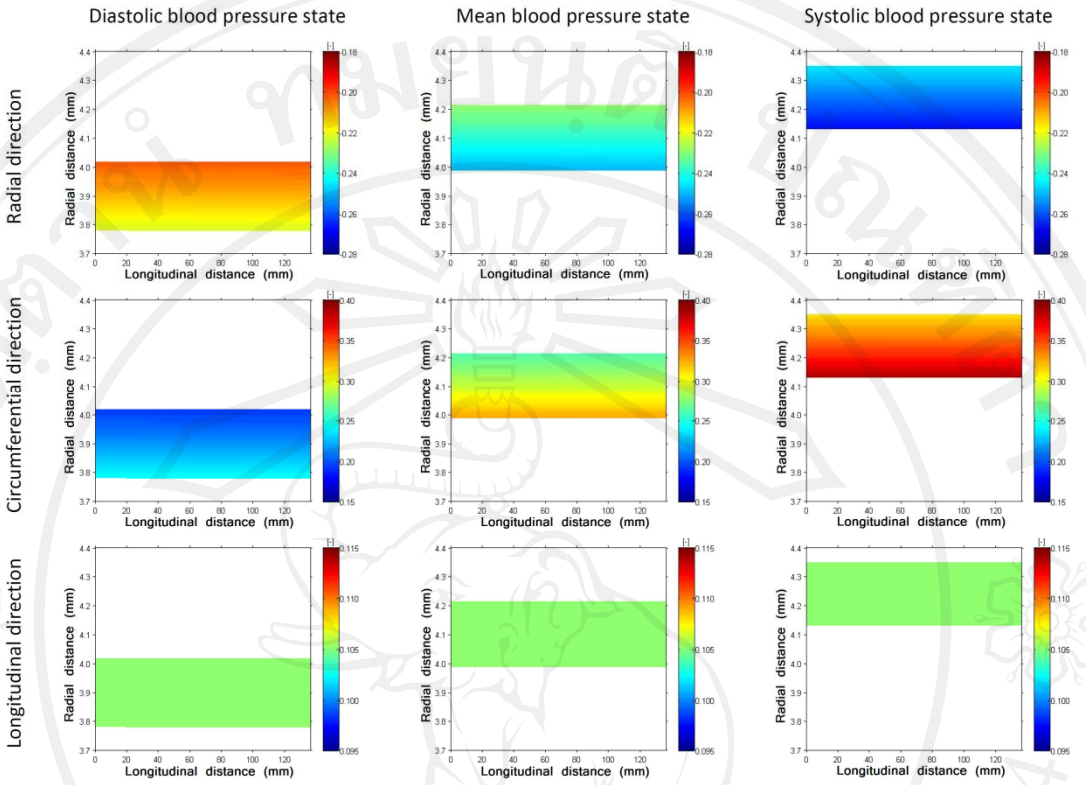

Figure 4.20 Capture images of principal Green-Lagrange strains distributions across the $r-z$ plane deformed arterial wall in radial direction (1st row), circumferential direction (2nd row) and longitudinal direction (3rd row) at DBP of 69.61 mmHg (1st column), MBP of 89.25 mmHg (2nd column) and SBP of 128.41 mmHg (3rd column) obtained from the model

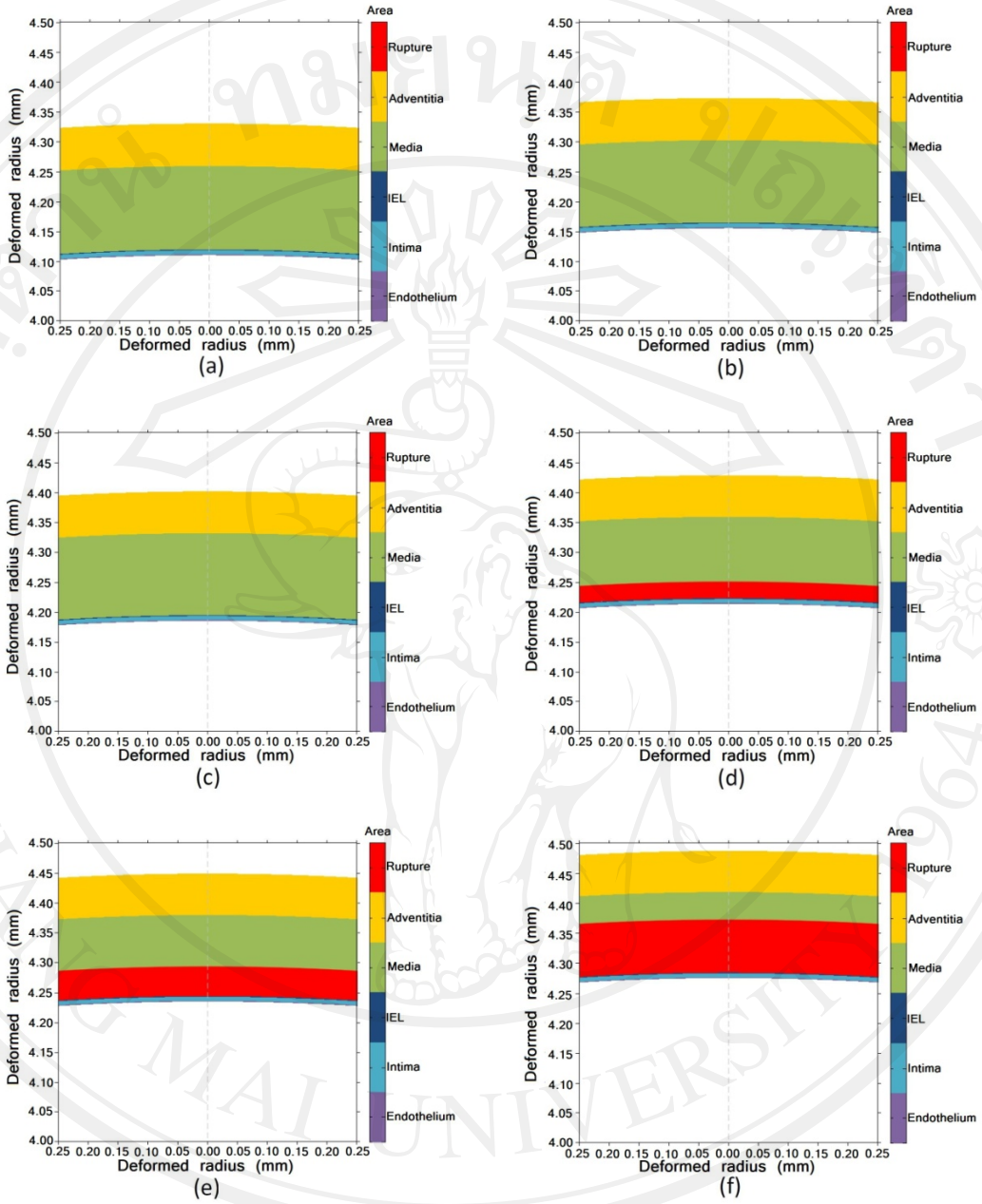

Figure 4.21 Rupture area of arterial wall by using stress and strain as a criterion. (a) through (f) illustrate rupture area in $r-\theta$ plane at luminal pressure of 120, 140, 160, 180, 200 and 250 mmHg, respectively. There are five colours to identify no rupture area, i.e. violet for endothelium, light blue for intima, dark blue for internal elastic lamina (IEL), green for media and yellow for adventitia. Wherever area that ruptures, red colour is represented.

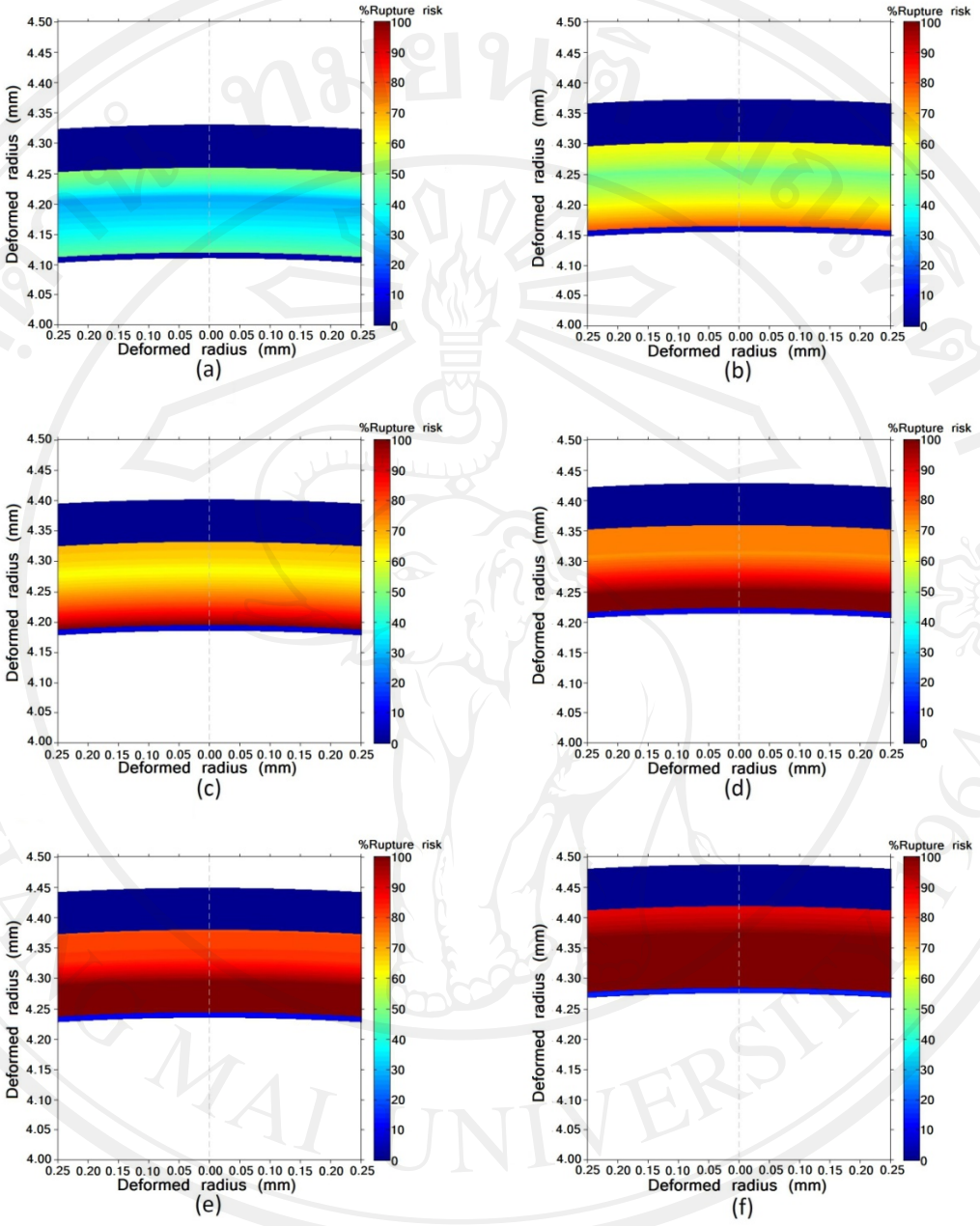

Figure 4.22 Percentage of rupture risk of arterial wall respected to physiological pressure of 100 mmHg by using stress and strain as a criterion. (a) through (f) illustrate the percentage of rupture risk in $r-\theta$ plane at luminal pressure of 120, 140, 160, 180, 200 and 250 mmHg, respectively.

As illustrated in Figure 4.20, magnitude of principal Green-Lagrange strains of normal human artery in radial and circumferential directions are in range of 0.20-0.27 and 0.19-0.39, respectively and in longitudinal direction is equal to 0.1050. The principal Green-Lagrange strain distributions in radial and circumferential directions represents higher magnitude at the inside walls and continuously decreases to lower magnitude at the outside wall. The negative value of strain in radial direction means that the thickness of arterial wall is reduced from the reference configuration and from the results it could be seen that arterial wall is thinner while the luminal pressure increased. By constant strain in longitudinal direction, the strain distribution in circumferential direction is positive value that means periphery of arterial wall increased to preserve its volume. At certain longitudinal position, the continuities of the strains distributions in all directions are obtains because continuous body of vascular is assumed.

Distributions of the stress and strain in longitudinal direction are analyzed from Newtonian blood flow. There are not clearly seen small variations of stresses and strains from inlet to outlet of the vessel which resulting from viscosity of blood in Figure 4.19 and Figure 4.20. The higher stresses and strains occur at the inlet where higher luminal pressure.

4.4. Effect of luminal pressure on rupture risk of aorta: case of multilayer aorta

The pressure load or stress acted on inside surface of arterial wall, the associated strain increase continually to the point of failure. In this study, the local failure is defined global failure or rupture since it is the beginning of completed failure.

It is difficult to separate responses of arterial wall resulting from stress and strain since both of stress and stain are significant in showing the characteristics of the material of the vessel. Hence, it is difficult to change one thing without affecting another. Figure 4.21 illustrates the result of rupture area by both of stress and strain as criterion.

Table 4.5 Levels of luminal pressure affecting arterial failure

Figure	Level	Luminal pressure, LP (mmHg)	Maximum percentage of rupture risk
4.21f, 4.22f	Beyond physiological pressure	200< LP ≤ 250	100 (Rupture propagation but no final failure)
4.21d-e 4.22d-e	Severe pressure	160< LP ≤ 200	100 (Rupture initiation and propagation at LP about 180 mmHg)
4.21c, 4.22c	High pressure	140< LP ≤ 160	< 100
4.21b, 4.22b	Moderate pressure	120< LP ≤ 140	< 80
4.21a. 4.22a	Normal pressure	0 ≤ LP ≤ 120	< 50

Therefore, from our result shown in Figure 4.21 the rupture characteristics could be qualitatively interpreted. The failure process could be separated into two regimes, failure initiation and failure propagation. There is no final failure found in domain of present study. The existence and extend of these failure initiation and propagation depend on the pressure or stress which relates to arterial geometry or

strain by the mechanics properties of each the arterial layer. It could be seen that the rupture occurs in circumferential around the arterial wall and the rupture initiates tear at inside medial surface of artery and extend over a small percentage of the failure surface. Moreover, the rupture propagates from inside medial surface toward to the outside surface.

In order to quantitatively interpret effect of pressure on arterial failure, percentage of rupture risk is performed. The result of percentage of rupture risk is shown in Figure 4.22. From this result level of pressure affecting to arterial failure could be divided into five ranges. First, normal pressure level is when the pressure is lower than 120 mmHg. In range of normal pressure level, it is found that maximum percentage of rupture risk does not exceed 50% (Figure 4.22a). The second level, moderate pressure level is when the pressure in range between 120 mmHg and 140 mmHg. At moderate pressure level, maximum percentage of rupture risk is much greater but does not greater than 80% (Figure 4.22b). Next, high pressure level is when the pressure in range between 140 mmHg and 160 mmHg. In this level of pressure, maximum percentage of rupture risk is quite high but does not reach to the level that rupture occurs (Figure 4.22c). The rupture initiation and propagation occur in severe pressure level which between 160 mmHg and 200 mmHg (Figure 4.22d and Figure 4.22e) by the rupture initiation occurs at pressure about 180 mmHg. Beyond physiological pressure level which is over than 200 mmHg, rupture area continuously increases but final failure has not found although the pressure as high as 250 mmHg (Figure 4.22f).